Coupled spin and electron-phonon interaction at the Tl/Si(111) surface from relativistic first-principles calculations

Peio Garcia-Goiricelaya, Idoia G. Gurtubay, and Asier Eiguren

Materia Kondentsatuaren Fisika Saila, University of the Basque Country UPV/EHU, 48080 Bilbao, Basque Country, Spain
and Donostia International Physics Center (DIPC), Paseo Manuel de Lardizabal 4, 20018 Donostia-San Sebastián, Spain

We investigate the role played by the electron spin and the spin-orbit interaction in the exceptional electron-phonon coupling at the Tl/Si(111) surface. Our first-principles calculations demonstrate that the particular spin pattern of this system dominates the whole low-energy electron-phonon physics, which is remarkably explained by forbidden spin-spin scattering channels. In particular, we show that the strength of the electron-phonon coupling appears drastically weakened for surface states close to the $\overline{K}$ and $\overline{K'}$ valleys, which is unambiguously attributed to the spin polarization through the associated modulation due to the spinor overlaps. However, close to the $\overline{\Gamma}$ point, the particular spin pattern in this area is less effective in damping the electron-phonon matrix elements, and the result is an exceptional strength of the electron-phonon coupling parameter $\lambda \sim 1.4$. These results are rationalized by a simple model for the electron-phonon matrix elements including the spinor terms.

In metals, the charge and spin transport, heat capacity, and many other thermodynamical properties, even superconductivity [1,2], are strongly influenced by the low-energy dynamics of the so-called quasiparticles. Quasiparticles incorporate the many-body interactions in an approximate way by treating the interacting particles as dressed particles with modified or renormalized properties [3,4]. Electron-phonon dynamics is particularly important in the low-energy domain, and effective masses and transport coefficients are determined mainly by this interaction in clean samples. Initiated by Migdal [5] and Engelsberg and Schrieffer [6], the Green's function perturbation theory has been successful in describing the realistic properties of materials in combination with *ab initio* techniques, even with a high predictive power [7]. The electron-phonon interaction has been investigated systematically in the bulk and surface systems, where it has been established that, as a general rule, the electron-phonon coupling is enhanced [8–10]. Furthermore, in low-dimensional systems, the spin-orbit (SO) coupling, far from being a mere relativistic correction, introduces important qualitative changes in the properties of materials, such as the generation of spin-split and spin-polarized electronic states, even in nominally nonmagnetic systems [11]. Likewise, the SO interaction is responsible for the existence of an entirely new quantum state of matter, which is characterized by its phase-space topology and exhibits exceptional transport properties at the edges of these materials [12]. Therefore, understanding the low-energy charge and spin-coupled dynamics in two-dimensional (2D) systems with strong SO coupling is of capital importance and a very active research front at the moment [13–15]. The coexistence of SO coupling and electron-phonon coupling has been studied considering instructive model theoretical treatments combining the Rashba SO term and the Fröhlich and Holstein term, revealing an intricate spin-dependent polaronic spectral function [16] and the impact of the singularity by the Rashba coupling on the electron density of states [17], among

other interesting phenomena associated with the relativistic corrections. Examples such as the valley-dependent electron-phonon coupling of transition-metal dichalcogenides [18] and the absence of backscattering in topological surface states [19] illustrate some important aspects related to spin polarization in the presence of electron-phonon coupling.

In this Rapid Communication, we investigate the electron-phonon dynamics at the Tl/Si(111) surface, keeping the full spin and momentum dependence of the electron-phonon matrix elements and allowing us to focus on the precise role played by the electron spin polarization. The Tl/Si(111) shows a very peculiar spin texture [20,21] and its band structure combines an in-plane rotational spin for the occupied surface states and a (collinear spin) valley pattern for the unoccupied ones. Therefore, the geometry of the electron-phonon coupling is radically different for the occupied and unoccupied spin-split surface states, but both energy regions should be accessible under doping. We analyze the energy and momentum dependence of the mass enhancement parameter for low-energy surface states, below and above the Fermi level, and we find a remarkable strength of the electron-phonon coupling. Moreover, in order to clarify the role of the spin polarization, we fix the electron momentum $\mathbf{k}$ at some representative points, and break up the $\mathbf{q}$-dependent contributions from the entire Brillouin zone, which allows us to correlate the results with the spin pattern of this surface. An extreme example illustrating how the spin structure enters the electron-phonon physics occurs when a phonon with momentum $\mathbf{q}$ connects two points of the surface Brillouin zone (SBZ) with orthogonal spin states causing an almost perfect extinction of the electron-phonon scattering. This picture applies perfectly for the unoccupied part of the band structure, as this area shows an ideal valley arrangement. However, the spin exclusion mechanism described above is not enough to weaken the exceptional magnitude of the electron-phonon interaction in the case of the occupied surface bands.

The Tl/Si(111) surface was simulated considering a slab consisting of ten silicon layers with a thallium monolayer on one termination of the slab (see Refs. [20,21] for a sketch of the structure). The silicon dangling bonds at the other end of the slab were saturated by inserting a single hydrogen coverage as in Refs. [20,21]. First-principles computations were performed using noncollinear density functional theory (DFT) [22,23] and density functional perturbation theory (DFPT) [24] approaches with fully relativistic norm-conserving pseudopotentials [25] as implemented in the QUANTUM ESPRESSO package [26–28] and using the Perdew-Burke-Ernzerhof generalized gradient approximation (PBE-GGA) parametrization [29] for the exchange-correlation energy. All atomic forces were relaxed up to at least 10^{-5} Ry/a.u. We used a 24×24 Monkhorst-Pack grid for self-consistent electronic calculations, while phonon modes were calculated in a coarse 8×8 q-point mesh. The SBZ integrals involved in the computation of the electron-phonon coupling were evaluated in very dense (10^6) k and q grids by means of a Wannier interpolation scheme [30,31]. In the Wannier procedure we included the four surface bands involved in the physical problem. Electron-phonon matrix elements were calculated considering spinor wave functions.

Figure 1 shows the electronic structure of the Tl/Si(111) surface. The black solid and red dashed lines show the scalar (i.e., without SO coupling) and fully (i.e., spin-split) relativistic surface state results, respectively. The left-hand sides of Figs. 1(a) and 1(b) display the electron surface band structure with respect to the Fermi level [dotted black line in Fig. 1(a)] in the eV and meV range, respectively, while those on the right-hand side represent the corresponding density of states (DOS). The silicon bulk band projection is illustrated by the gray shaded area. These calculations show an excellent agreement with photoemission measurements [32–34] and previous theoretical studies [20,21]. When SO effects are included, the highest occupied S_1 scalar surface band spin-splits into the $S_1^\uparrow$ and $S_1^\downarrow$ bands, dominating the low-energy region close to the Fermi level. The lowest unoccupied S_2 surface band, on the other hand, spin-splits into $S_2^\uparrow$ and $S_2^\downarrow$, yielding the strongest spin-split energy known in literature (~ 0.6 eV at $\overline{K}$). The inset of Fig. 1(b) shows the constant energy surfaces and contours corresponding to the scalar energies given by the dashed-dotted lines for three selected carrier momenta in the band structure plot: k_A and k_B for the occupied S_1 surface band, and k_C for the unoccupied S_2 band. While the S_2 surface band appears isotropic around $\overline{K}$ and $\overline{K'}$, the contour corresponding to the S_1 surface band presents a hexagonal (daisy-flower-like) anisotropy. The same holds for the spin-split $S_2^{\uparrow,\downarrow}$ and $S_1^{\uparrow,\downarrow}$ surface bands, respectively, except that the latter will show a double concentric structure, as shown in the right-hand panel of Fig. 4(c). The DOS corresponding to the scalar S_1 surface band exhibits a single one-dimensional (1D)-like singularity at the top of the band. For the spin-polarized surface bands ($S_1^{\uparrow,\downarrow}$), each state shows this singularity. Obviously, the electron-phonon coupling is enhanced close to the phase space connected to these singularities, as it will be demonstrated shortly.

Figure 2 displays the phonon dispersion at the Tl/Si(111) surface for the complete energy range [Fig. 2(a)] and the 0–9 meV range [Fig. 2(b)], the latter showing only the three
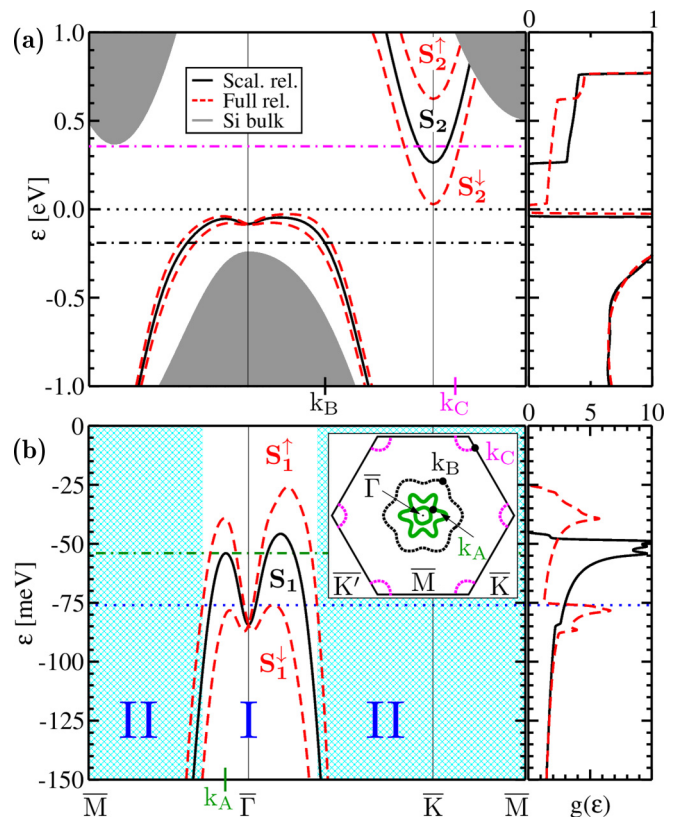

FIG. 1. Electron band structure for the (a) eV and (b) meV range of energy (left) and the corresponding DOS (right) of the Tl/Si(111) surface. The scalar and fully relativistic calculations are represented by black solid and red dashed lines, respectively. The gray shaded area in (a) is the bulk band projection. The inset in (b) shows the energy contour of the highest occupied band at $\mathbf{k} = k_A$ and $\mathbf{k} = k_B$ and the lowest unoccupied band at $\mathbf{k} = k_C$ in the scalar case. The corresponding energy levels are plotted by dashed-dotted lines in (a) for k_B (black) and k_C (magenta) and in (b) for k_A (green).

low-energy acoustic surface phonon modes, which correspond fundamentally to localized vibrations connected to Tl displacements. Ordered by increasing energy, we label these modes according to their polarization near $\overline{\Gamma}$, which correspond essentially to the longitudinal (L), shear horizontal (SH), and the Rayleigh mode (RM). These will be the most relevant modes for the coupling with the electron surface states. We proceed now to analyze the electronic energy ($E_F = \varepsilon_i^{\mathbf{k}}$) and momentum ($\mathbf{k}$) dependence of the electron-phonon mass enhancement parameter (λ) defined as

$$\lambda_{\mathbf{k},i} = \sum_{\mathbf{k}'j\nu} \frac{\left| g_{ij}^\nu(\mathbf{k},\mathbf{k}') \right|^2}{\omega_\nu^{\mathbf{k}-\mathbf{k}'}} \delta\left(\varepsilon_i^{\mathbf{k}} - \varepsilon_j^{\mathbf{k}'} \pm \omega_\nu^{\mathbf{k}-\mathbf{k}'} \right). \quad (1)$$

In Eq. (1), $g_{ij}^\nu(\mathbf{k},\mathbf{k}')$ denote the electron-phonon matrix elements, $\varepsilon_i^{\mathbf{k}}$ are the bare electron band energies, and $\omega_\nu^{\mathbf{k}-\mathbf{k}'}$ represent the phonon energies for momentum $\mathbf{q} = \mathbf{k} - \mathbf{k}'$. The λ parameter is one of the most representative magnitudes of the strength of the electron-phonon coupling and strictly speaking is defined as $\lambda_{\mathbf{k},i} = -\mathrm{Re}[\partial \Sigma_{\mathbf{k},i}(\omega)/\partial \omega]_{\omega=E_F}$, where $\Sigma_{\mathbf{k},i}(\omega)$ is the electron self-energy [1]. Figure 3(a) shows the calculated
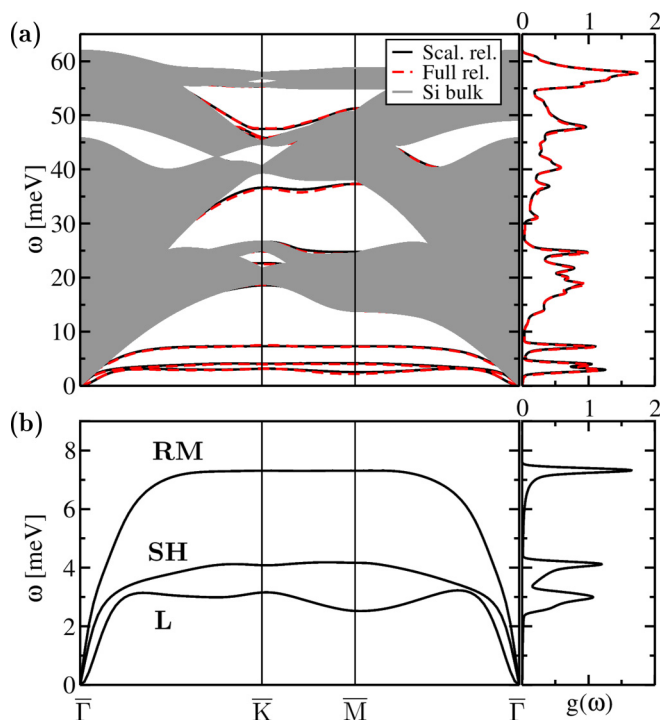
FIG. 2. (a) Phonon dispersion relation (left) and corresponding phonon density of states (PHDOS) (right) of the Tl/Si(111) surface. (b) Vibrational spectrum for the three acoustic modes. The scalar and fully relativistic calculations are represented by solid black and dashed red lines, respectively. The shaded gray area in (a) is the bulk band projection.

$\lambda_{\mathbf{k},i}$ for the unoccupied scalar S_2 surface band (solid black) and for the spin-split $S_2^\downarrow$ surface band (dashed red), as a function of the electron momentum around the valley $\overline{K}$, and along the high-symmetry directions $\overline{\Gamma K}$ and $\overline{KM}$.[1] As mentioned before, the three low-energy phonon modes contribute to 98% of the coupling strength. The quantitative and qualitative differences between the scalar and fully relativistic results are striking. At $\overline{K}$, $\lambda_{\overline{K},S_2^\downarrow}$ vanishes for the spin-split band, which is in complete contrast with the scalar case, where we find $\lambda_{\overline{K},S_2} = 0.45$. Moving away from the center of the valley $\overline{K}$, our calculations show that the momentum-resolved mass enhancement parameter is about one order of magnitude stronger for the scalar relativistic band. The reason for the steplike behavior of the latter is that, in the immediate vicinity of the bottom of the valley, no phonon-emitting electron scattering channel is energetically accessible and only the hole-phonon processes are possible, which means that solely the term $\delta(\varepsilon_i^{\mathbf{k}} - \varepsilon_j^{\mathbf{k}'} + \omega_\nu^{\mathbf{k}-\mathbf{k}'})$ contributes to Eq. (1). However, when the difference between the energy $\varepsilon_i^{\mathbf{k}}$ and that of the bottom of the valley equals, or is greater than, the smallest surface phonon energy, phonon-emitting electron scattering events $[\delta(\varepsilon_i^{\mathbf{k}} - \varepsilon_j^{\mathbf{k}'} - \omega_\nu^{\mathbf{k}-\mathbf{k}'})]$ are also allowed and $\lambda_{\mathbf{k},S_2}$ reaches a value of 0.9. As momentum and energy increases, the

---

[1]For the spin-split $S_2^\uparrow$ band, the coupling with bulk states dominates and it is outside the scope of this work.
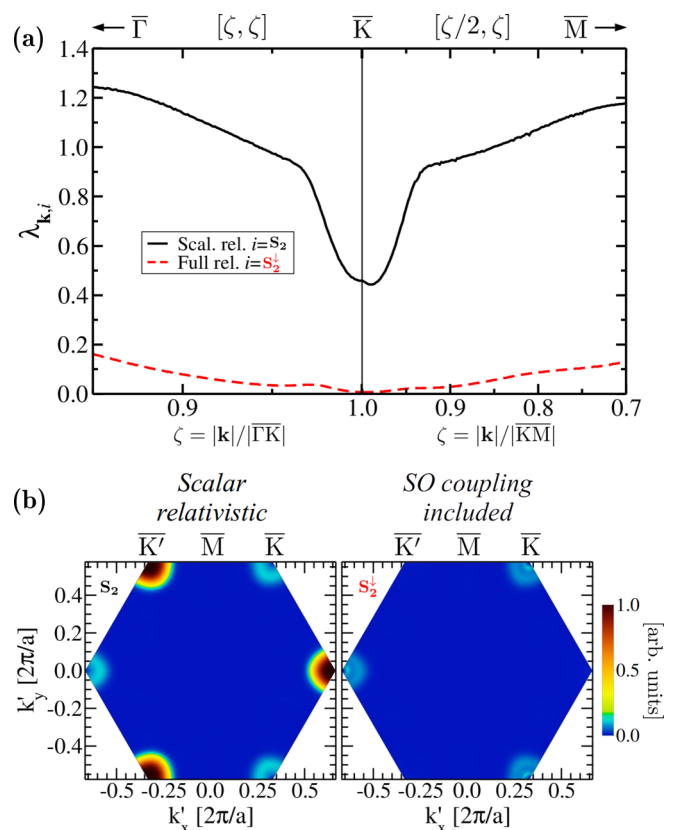

FIG. 3. (a) Momentum-dependent electron-phonon $\lambda_{\mathbf{k},i}$ parameter for the lowest unoccupied band around $\overline{K}$ for the scalar relativistic S_2 surface band (solid black) and for the spin-split $S_2^\downarrow$ surface band (dashed red). (b) $\mathbf{k}'$ momentum-resolved contributions to $\lambda_{\mathbf{k}=\overline{K},i}$ [see the integrand of Eq. (1)] within the SBZ for the scalar S_2 (left) and spin-split $S_2^\downarrow$ (right) surface bands.

coupling strength grows smoothly following the same trend as the DOS in Fig. 1(a). For the spin-split $S_2^\downarrow$ surface states, $\lambda_{\mathbf{k},S_2^\downarrow}$ is practically zero close to the bottom of the valley and, as energy increases, it grows up to values not larger than 0.2. Figure 3(b) helps to understand the difference between the spin-split and scalar results. The left (right) panel shows the contributions from each point in the SBZ to the calculation of $\lambda_{\mathbf{k},i}$ by means of Eq. (1) for the scalar S_2 (spin-split $S_2^\downarrow$) case when the electron momentum is fixed to be $\mathbf{k} = \overline{K}$. The obvious difference appears at $\mathbf{k}' = \overline{K'}$, where the contribution is maximum in the scalar relativistic case but results to be negligible in the fully relativistic one. Actually, spin-split unoccupied surface spinor states have surface-perpendicular opposite spin polarizations at $\overline{K}$ and $\overline{K'}$ [20,21,32–34], and therefore intervalley ($\overline{K} \to \overline{K'}$) scattering via phonon emission is forbidden, which is in complete contrast with the scalar case where this scattering channel is perfectly accessible. Intravalley ($\overline{K} \to \overline{K}$ or $\overline{K'} \to \overline{K'}$) decay channels, on the other hand, are allowed in both scalar and fully relativistic cases, although with a smaller probability [see the color scale in Fig. 3(b)].

Figure 4(a) shows the momentum dependence of the λ parameter for the occupied surface states close to $\overline{\Gamma}$ in the scalar S_1 band (solid black), and in the spin-split $S_1^\downarrow$ (dotted red) and $S_1^\uparrow$ (dashed red) bands, along the high-symmetry directions
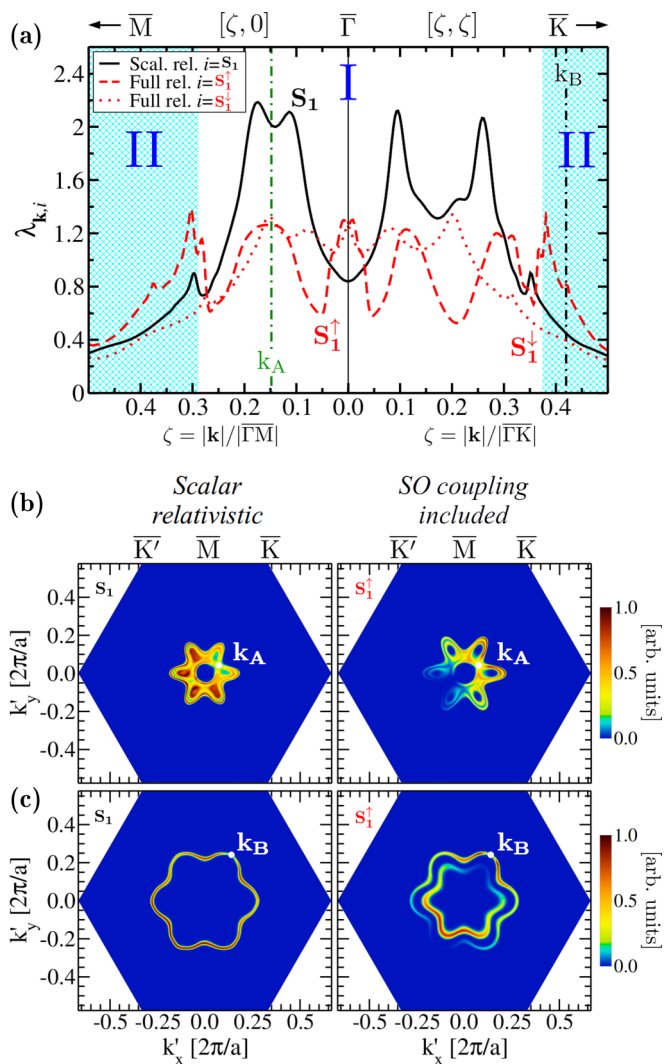
FIG. 4. (a) Momentum-dependent electron-phonon $\lambda_{\mathbf{k},i}$ parameter for the highest occupied bands around $\overline{\Gamma}$. The solid black line displays the result for the scalar S_1 surface band while dashed and dotted red lines show the spin-split $S_1^\uparrow$ and $S_1^\downarrow$ results, respectively. Regions I and II correspond to the ones in Fig. 1. (b) and (c) show the $\mathbf{k}'$ momentum-resolved contributions to $\lambda_{\mathbf{k},i}$ [see the integrand of Eq. (1)] within the SBZ for the scalar S_1 (left) and spin-split $S_1^\uparrow$ (right) surface bands when $\mathbf{k} = k_A$ (region I) and $\mathbf{k} = k_B$ (region II), respectively. k_A and k_B are shown in Fig. 1.

$\overline{\Gamma M}$ and $\overline{\Gamma K}$. In this case, 95% of the contribution comes from the three acoustic phonon modes. We can distinguish two different regimes in Fig. 4(a): In region II, the scalar and fully relativistic results are similar, which is in contrast with region I, where even if the fully relativistic electron-phonon coupling strengths are damped by up to a factor of 3 compared to the scalar results, we still find values of λ as large as 1.4.[2] The phase space of regions I and II is also displayed in the patterned blue areas of the surface band

structure of Fig. 1(b): Region I above the horizontal blue dotted line corresponds to the phase space of the spin-split $S_1^\uparrow$ surface states where only intraband scattering processes are allowed, while below this line and in region II, intraband or and interband processes are accessible for both $S_1^\uparrow$ and $S_1^\downarrow$. Figure 4(b) shows the momentum-resolved contributions to $\lambda_{\mathbf{k},i}$ [Eq. (1)] for the scalar S_1 (left) and spin-split $S_1^\uparrow$ (right) surface bands for $\mathbf{k} = k_A$ belonging to region I [see Fig. 1(b)]. Figure 4(c) gives the corresponding results for $\mathbf{k} = k_B$ within region II. Clearly, the contributions shown in the left and right panels of Fig. 4(c) are very similar, whereas Fig. 4(b) shows that they are strongly weakened when SO interaction is included. This is easily understood in terms of spin-state overlaps. Let us recall that occupied spin-split surface bands have a Rashba-like [35] chiral spin polarization [20,21] on the surface plane near $\overline{\Gamma}$. In the Rashba model, the spinor overlaps between two different states within the same spin-split band (intraband) appear modulated appropriately by $(1 + \cos\theta)/2$, θ being the angle between the initial and final momentum of the electron. Yet, when the overlap happens between two states belonging to different spin-split bands (interband), overlaps vary as $(1 - \cos\theta)/2$, since the spin is polarized in opposite directions in each band. Therefore, in region II, where both interband and intraband channels are allowed, the results are qualitatively similar to the spin-degenerate case [Fig. 4(c)]. However, in region I, where only intraband contributions are accessible for the $S_1^\uparrow$ band, the matrix elements are reduced by $(1 + \cos\theta)/2$, as shown in Fig. 4(b). In the case of $S_1^\downarrow$, although both intra- and interband scattering processes are allowed, $\lambda_{\mathbf{k},S_1^\downarrow}$ still shows a noticeable attenuation in region I compared to the scalar case. This is attributed to the difference between the scalar and spin-split electronic density of states.

In summary, we demonstrate the fundamental role played by the electron spin and the relativistic effects on the dynamics of surface electrons at the Tl/Si(111) surface. We have calculated the state-dependent electron-phonon mass enhancement parameter and shown that the spin polarization of the surface states enters in a decisive way by modulating the electron-phonon matrix elements which we have demonstrated unambiguously by representing the (squared) matrix elements though the entire Brillouin zone. We show that the electron-phonon coupling appears strongly weakened for the unoccupied bands (S_2) in this surface, as these bands are arranged in a collinear spin valley structure. More interestingly, while the restriction imposed by the spin polarization should also apply to the occupied surface bands (S_1), the strength of the coupling remains remarkably high ($\lambda \sim 1.4$). The strong-coupling regime reached in the presence of SO interaction is a theoretically challenging problem since, for instance, spin-polarized polaronlike states may be favored, which clearly demands a deeper understanding of the transport properties in this surface. We believe that this work should stimulate further experimental and theoretical investigations in this research front.

---

[2]A simple McMillan formula estimate gives a superconducting transition temperature of $T_c \approx 7$K for the relativistic case but a strong coupling analysis is in order.

[1] G. Grimvall, *The Electron-Phonon Interaction in Metals*, Se-lected Topics in Solid State Physics (North-Holland, New York, 1981).

[2] G. D. Mahan, *Many-Particle Physics*, 3rd ed. (Springer, New York, 2000).

[3] L. Hedin and S. Lundqvist, *Solid State Physics*, Vol. 23 (Academic, New York, 1969), pp. 1–181.

[4] P. Nozières, *Theory of Interacting Fermi Systems* (W. A. Benjamin, New York, 1964).

[5] A. B. Migdal, Zh. Eksp. Teor. Fiz. **34**, 1438 (1958) [Sov. Phys. JETP **7**, 996 (1958)].

[6] S. Engelsberg and J. R. Schrieffer, Phys. Rev. **131**, 993 (1963).

[7] F. Giustino, Rev. Mod. Phys. **89**, 015003 (2017).

[8] E. Plummer, J. Shi, S.-J. Tang, E. Rotenberg, and S. Kevan, Prog. Surf. Sci. **74**, 251 (2003).

[9] P. Hofmann, I. Y. Sklyadneva, E. D. L. Rienks, and E. V. Chulkov, New J. Phys. **11**, 125005 (2009).

[10] A. Eiguren, B. Hellsing, F. Reinert, G. Nicolay, E. V. Chulkov, V. M. Silkin, S. Hüfner, and P. M. Echenique, Phys. Rev. Lett. **88**, 066805 (2002).

[11] J. I. Pascual, G. Bihlmayer, Y. M. Koroteev, H.-P. Rust, G. Ceballos, M. Hansmann, K. Horn, E. V. Chulkov, S. Blügel, P. M. Echenique, and P. Hofmann, Phys. Rev. Lett. **93**, 196802 (2004).

[12] M. Z. Hasan and C. L. Kane, Rev. Mod. Phys. **82**, 3045 (2010).

[13] G. Bihlmayer, O. Rader, and R. Winkler, New J. Phys. **17**, 050202 (2015).

[14] A. Manchon, H. C. Koo, J. Nitta, S. M. Frolov, and R. A. Duine, Nat. Mater. **14**, 871 (2015).

[15] E. I. Rashba, J. Phys.: Condens. Matter **28**, 421004 (2016).

[16] L. Covaci and M. Berciu, Phys. Rev. Lett. **102**, 186403 (2009).

[17] E. Cappelluti, C. Grimaldi, and F. Marsiglio, Phys. Rev. B **76**, 085334 (2007).

[18] N. F. Hinsche, A. S. Ngankeu, K. Guilloy, S. K. Mahatha, A. Grubišić Čabo, M. Bianchi, M. Dendzik, C. E. Sanders, J. A. Miwa, H. Bana, E. Travaglia, P. Lacovig, L. Bignardi, R. Larciprete, A. Baraldi, S. Lizzit, K. S. Thygesen, and P. Hofmann, Phys. Rev. B **96**, 121402(R) (2017).

[19] R. Heid, I. Y. Sklyadneva, and E. V. Chulkov, Sci. Rep. **7**, 1095 (2017).

[20] J. Ibañez-Azpiroz, A. Eiguren, and A. Bergara, Phys. Rev. B **84**, 125435 (2011).

[21] J. Lafuente-Bartolome, I. G. Gurtubay, and A. Eiguren, Phys. Rev. B **96**, 035416 (2017).

[22] P. Hohenberg and W. Kohn, Phys. Rev. **136**, B864 (1964).

[23] W. Kohn and L. J. Sham, Phys. Rev. **140**, A1133 (1965).

[24] S. Baroni, S. de Gironcoli, A. Dal Corso, and P. Giannozzi, Rev. Mod. Phys. **73**, 515 (2001).

[25] D. R. Hamann, Phys. Rev. B **40**, 2980 (1989).

[26] L. Kleinman, Phys. Rev. B **21**, 2630 (1980).

[27] A. D. Corso and A. Mosca Conte, Phys. Rev. B **71**, 115106 (2005).

[28] P. Giannozzi, S. Baroni, N. Bonini, M. Calandra, R. Car, C. Cavazzoni, D. Ceresoli, G. L. Chiarotti, M. Cococcioni, I. Dabo, A. D. Corso, S. de Gironcoli, S. Fabris, G. Fratesi, R. Gebauer, U. Gerstmann, C. Gougoussis, A. Kokalj, M. Lazzeri, L. Martin-Samos *et al.*, J. Phys.: Condens. Matter **21**, 395502 (2009).

[29] J. P. Perdew, K. Burke, and M. Ernzerhof, Phys. Rev. Lett. **77**, 3865 (1996).

[30] F. Giustino, J. R. Yates, I. Souza, M. L. Cohen, and G. Louie, Phys. Rev. Lett. **98**, 047005 (2007).

[31] A. Eiguren and C. Ambrosch-Draxl, Phys. Rev. B **78**, 045124 (2008).

[32] K. Sakamoto, T.-H. Kim, T. Kuzumaki, B. Müller, Y. Yamamoto, M. Ohtaka, J. R. Osiecki, K. Miyamoto, Y. Takeichi, A. Hara-sawa, S. D. Stolwijk, A. B. Schmidt, J. Fujii, R. I. G. Uhrberg, M. Donath, H. W. Yeom, and T. Oda, Nat. Commun. **4**, 2073 (2013).

[33] K. Sakamoto, T. Oda, A. Kimura, K. Miyamoto, M. Tsujikawa, A. Imai, N. Ueno, H. Namatame, M. Taniguchi, P. E. J. Eriksson, and R. I. G. Uhrberg, Phys. Rev. Lett. **102**, 096805 (2009).

[34] S. D. Stolwijk, A. B. Schmidt, M. Donath, K. Sakamoto, and P. Krüger, Phys. Rev. Lett. **111**, 176402 (2013).

[35] Y. A. Bychkov and E. I. Rashba, Sov. Phys. - JETP Lett. **39**, 78 (1984).